Cytometry Part A 69A:735–747 (2006)

Spectral Imaging: Principles and Applications

Yuval Garini,[1,3]* Ian T. Young,[1] and George McNamara[2]

[1]Quantitative Imaging Group, Faculty of Applied Sciences, Delft University of Technology, Delft, The Netherlands
[2]Division of Cancer Immunotherapeutics and Tumor Immunology, City of Hope National Medical Center, California, USA
[3]Department of Physics, Bar-Ilan University, Ramat-Gan, Israel

Received 11 November 2005; Revision Received 5 May 2006; Accepted 8 May 2006

Background: Spectral imaging extends the capabilities of biological and clinical studies to simultaneously study multiple features such as organelles and proteins qualitatively and quantitatively. Spectral imaging combines two well-known scientific methodologies, namely spectroscopy and imaging, to provide a new advantageous tool. The need to measure the spectrum at each point of the image requires combining dispersive optics with the more common imaging equipment, and introduces constrains as well.
Methods and Results: The principles of spectral imaging and a few representative applications are described. Spectral imaging analysis is necessary because the complex data structure cannot be analyzed visually. A few of the algorithms are discussed with emphasis on the usage for different experimental modes (fluorescence and bright field). Finally, spectral imaging, like any method, should be evaluated in light of its advantages to specific applications, a selection of which is described.
Conclusions: Spectral imaging is a relatively new technique and its full potential is yet to be exploited. Nevertheless, several applications have already shown its potential. © 2006 International Society for Analytical Cytology

Key terms: spectral imaging; multicolor microscopy; image analysis; spectral unmixing; linear decomposition

Spectral imaging combines spectroscopy and imaging. Each of these fields is well developed and is being used intensively in many fields including the life sciences. The combination of these two is, however, not trivial, mainly because it requires creating a three-dimensional (3D) data set that contains many images of the same object, where each one of them is measured at a different wavelength. It also means that the total acquisition time is long, which stands in contrast to the requirements of many bio-medical applications. Therefore, compromises must be made for high quality images in a limited amount of time.

For explaining the characteristics of spectral imaging, it is better to start with an introduction of the two elements of spectral imaging; imaging and spectroscopy.

IMAGING

Imaging is the science and technology of acquiring spatial and temporal data information from objects for the purpose of obtaining information. At this time, digital imaging is the most advanced and applicable method where data are recorded using a digital camera, such as a charged coupled device (CCD).

In biological studies, the images can be measured either by common optical methods such as optical microscopy or by more advanced methods that provides additional physical or chemical information about the objects; examples include optical coherence tomography and life-time imaging. Because of the broad usage of imaging, we limit the following discussion to optical microscopy, mainly in the visible-light range.

The quality of an image determines the amount of information that can be extracted from it and the following list describes the most common parameters that characterize the acquired images:

1. Spatial resolution determines the closest distinguishable features in the objects. It depends mainly on the wavelength (λ), the numerical aperture (NA) of the objective lens, the magnification, and the pixel size of the array-detector, usually a CCD camera. The latter two play a role because they determine the sampling frequency which must be sufficiently high to achieve full resolution. Spatial resolution also depends on the signal quality (1).
2. Lowest detectable signal depends on the quantum efficiency of the detector (the higher the better), the noise level of the system (the lower the better), the NA of the optics (the higher the better), and the quality of the optics. It is especially important in applications where the num-

Grant sponsors: Delft Inter-Faculty Research Center Life-Tech, Bsik Research Program Cyttron, Delft Research Program Life Science and Technology.
*Correspondence to: Yuval Garini.
E-mail: y.garini@tudelft.nl
Published online in Wiley InterScience (www.interscience.wiley.com).
DOI: 10.1002/cyto.a.20311

ber of photons is limited, or where the total time that is available for the measurement is limited (e.g., due to fluorescence quenching by oxygen or in live-cell imaging).

3. Dynamic range of the acquired data determines the number of different intensity levels that can be detected in an image. It depends on the maximal possible number of electrons at each pixel and on the lowest detectable signal (basically it is the ratio of these two values). If, however, the measured signal is low, so that the CCD well associated with a pixel is only partially filled, the dynamic range will be limited accordingly. As an example, if a CCD well is fulfilled to only 10% of its maximum capacity, the dynamic range will be reduced to 10% of its nominal value.

4. Field of view (FOV) determines the maximal area that can be imaged.

5. Other parameters include the exposure time range (usually determined by the detector) and the binning of CCD pixels to gain sensitivity (by trading-off spatial resolution).

See Table 1 for a summary and typical parameters values.

Excellent quality CCD's as well as photomultipliers and other light-detectors are now available. Nevertheless, even with an ideal detector with no noise at all, the light itself has intrinsic noise (shot noise) that cannot be avoided. If n photons have been counted, then shot noise, with its Poisson distribution, has a standard deviation of about $\sqrt{n}$. The signal-to-noise ratio (SNR) is proportional to $n/\sqrt{n} = \sqrt{n}$ and can only be improved by increasing the intensity, the exposure time, or both. At best, an imaging system is "shot-noise limited," which means that the quality of the detector is high enough so that the sensitivity of the system is limited by the shot-noise.

In actual measurements, there are many imperfections that reduce the quality of the image such as autofluorescence, non-specific staining, bleaching and others, but these should be distinguished from the physical limitations set by the electro-optical system itself and the nature of light.

Table 1
Characteristic parameters of a spectral imaging system. The "typical" value shows the common value that is achievable, but depends on the specific dispersion method that is used and the quality of the system elements (e.g. high NA objective lens, high quantum efficiency QE)

Category	Property	Typical
Imaging	Spatial resolution	250 nm (in plane) at $\lambda = 500$ nm
	Field of view	~50 μm (high magnification)
	Dynamic range	8–16 bits (256–65, 536 intensity levels)
	Lowest detectable signal	Shot-noise limited
Spectroscopy	Spectral resolution	1–20 nm (may depend on λ)
	Spectral range	400–900 nm

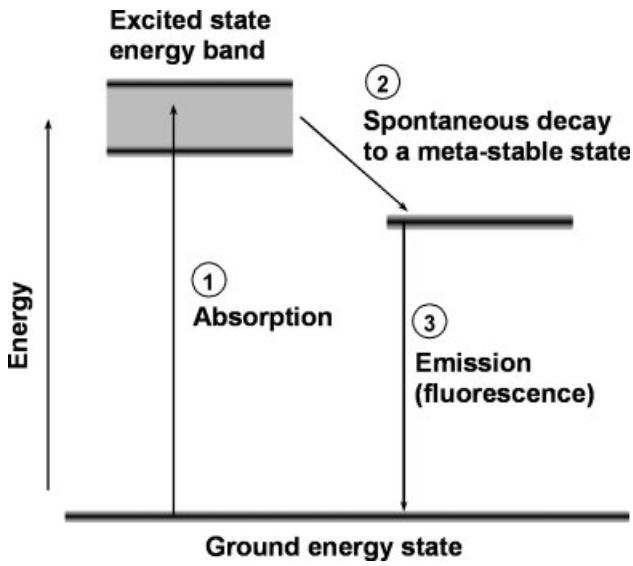

FIG. 1. A simplified energy-level diagram of a fluorescent molecule (1). Electrons are excited from the ground state to the excited band by absorbing a photon (2). The electrons decay rapidly to a meta-stable energy level (3). Electrons fall back to the ground state by emitting a photon with lower energy relative to the exciting photon.

SPECTROSCOPY

Spectroscopy is a term that is used to describe different phenomena, and we limit our discussion to optical spectroscopy, mainly in the visible light range. A spectrum is a collection of light intensities at different wavelengths. Spectroscopy, the science of acquiring and explaining the spectral characteristics of matter, is a broad, well established and old science. Newton described the dispersion of white light to its constituent colors (2,3) in 1666 and by 1900 the spectrograph, a system for measuring a spectrum, was widely used. Spectroscopy provided the spectrum of hydrogen that was explained by Balmer in 1885, which led in 1913 to the Böhr model of the atom (4), and finally to the development of quantum mechanics by Schrödinger in 1926 (5).

The structure of atoms and molecules is directly related to spectroscopy. The spectrum is a direct measurement of the energy levels of the detected structure (Fig. 1). Molecules (and atoms) have a specific energy-band structure. In an absorption process (which occurs in both bright-field and fluorescence microscopy), an electron is excited from the ground state to an excited energy band (1 in Fig. 1). In fluorescence, the electron rapidly decays to a meta-stable energy level (2 in Fig. 1). Then, light is emitted when the electron decays back to the ground state (3 in Fig. 1). The energy levels are intrinsic properties of the molecule, and the spectrum, therefore, provides a precise fingerprint of the molecule.

Even though this work focuses on the visible-light spectral range (which is relevant for the electronic transitions described earlier), the infrared spectrum (usually 2–20 μm) is also heavily used for measuring absorption by matter. The infrared light is much less energetic (an infrared

photon carries much less energy than in the visible range) and it can be absorbed by molecules and initiate a vibration and rotation of the atoms, sometimes called vibronic modes. The vibrations are specific to the inter-atomic bonds and therefore the infrared absorption of a molecule is an excellent fingerprint of its structure (6). Raman spectroscopy allows one to monitor the infrared absorption by performing the actual measurements in the visible light spectral range (7).

It is important to distinguish fluorescence and absorption processes. In fluorescence measurement (also luminescence and phosphorescence), fluorescent molecules (or other fluorescing entities) are attached to the objects, or the object itself is the source of light (such as chlorophyll or a fluorescent protein). In many cases there is a direct functional relationship between the concentration of fluorescent molecules and the amount of fluorescence intensity. At low concentrations this relationship is linear and therefore quantitative analysis is possible.

In fluorescence it is essential to distinguish the weak emitted light from the strong excitation light. This requires the use of color filters, excitation barrier filters, dichroic mirrors, and emission barrier filters that allows one to distinguish the two light sources. These filters must have adequate transmission ranges and high rejection ratios at the required wavelength and the spectrum that is measured is, therefore, usually different from the real emitted spectrum. Different effects such as saturation and bleaching may disrupt an expected linearity of the signal and should be tested for each specific case.

In bright-field microscopy, reflection microscopy, and scattering microscopy, the sample is illuminated with an external light source and the detector measures that very same light after interaction with the sample. Spectral analysis of the data must take into account the light source spectrum in order to accurately extract the desired spectrum. In bright-field microscopy, the measured signal may not be directly proportional to the concentration of the observed molecules but to its logarithm.

To measure a spectrum, the light is dispersed into its different wavelengths (or color) components and the intensity at each one is measured. There are different methods to disperse the light and almost all of them are used in various spectral imaging systems. Some of the important characteristics of a spectrum includes (see also Table 1):

1. The spectral resolution determines the closest wavelengths that can be distinguished.
2. The spectral range in which spectra can be measured.
3. The lowest detectable signal and dynamic range, which defines the smallest measurable signal and the number of distinguishable levels in a given measurement. These parameters also depend on the shape of the measured spectrum. A sharp laser line has a better detectable signal because the energy is concentrated at a single wavelength when compared to a broad spectrum with equal energy which is distributed over a large spectral range.

SPECTRAL IMAGING

Spectral imaging combines these two methodologies, spectroscopy and imaging. Whereas imaging provides the intensity at every pixel of the image, $I(x,y)$, and a typical spectrometer provides a single spectrum, $I(\lambda)$, a spectral image provides a spectrum at each pixel, $I(x,y,\lambda)$. This is a 3D data set and can be viewed as a cube of information. One can consider $I(x,y,\lambda)$ as either a collection of many images in which each one is measured at a different wavelength or as a collection of many spectral values at each pixel (Fig. 2).

REALIZATION OF SPECTRAL IMAGES

Spectral imaging requires the combination of a dispersive element (or method) for acquiring the spectral information with an imaging system. The data collected at each pixel is the intensity at each wavelength, $I(x,y,\lambda)$ (Fig. 2). When a 2D array detector is used (e.g., CCD), the spectral image cannot be acquired at once. If a lower-dimension detector, such as a line-detector or a single-point detector, is used then even more time will be required. This challenge has led to the development of different methods as described later.

Spectral imaging methods can be divided into the following methods: (1) Wavelength-scan methods that measure the images one wavelength at a time. (2) Spatial-scan methods that measure the whole spectrum of a portion of the image at a time and scan the image (e.g., line by line). (3) Time-scan methods that measure a set of images where each one of them is a superposition of spectral or spatial image information. At the end of the acquisition, the data is transformed to the actual spectral image (e.g., by Fourier methods). (4) Methods that measures the whole spectral image simultaneously, but compromise on the number of points in the spectrum, the FOV or spatial resolution.

If we assume that a spectral imaging system consists of ideal optical elements, the quality of the acquired data of a spectral image, at a given amount of time, depends only on the signal itself and on the simultaneous number of detector elements that collects information from the image; the larger the number, the faster the measurement.

Wavelength-Scan Methods

A simple method for measuring a spectral image is to use a set of color-filters (Fig. 3B), each of which transmits a narrow band wavelength (say a bandwidth of 10 nm). Such a system is inappropriate when a large number of wavelengths (filters) are required. It is practical only where a very small number of wavelengths are needed.

A more convenient way is to use variable-filters, which are more compact and robust. Three common variable filters include the circular-variable filter (CVF) (8) as shown in Figure 3A, liquid-crystal tunable filter (LCTF) (9) shown in Figure 3C, and acousto-optical tunable filter (AOTF) (10,11), as shown in Figure 3D. The CVF transmits a narrow-band light depending on the beam position on its surface (usually around a circular filter). The AOTF and LCTF are electro-optical components with no moving parts. The

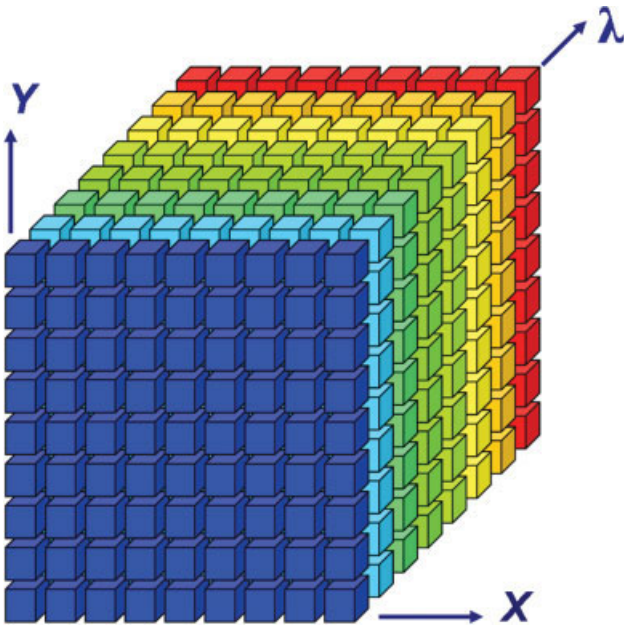

FIG. 2. Description of a spectral image data set. Each point in the cube represents a single number and the spectral image is described as $I(x,y,\lambda)$. It can be viewed either as an image $I(x,y)$ at each wavelength λ, or as a spectrum $I(\lambda)$ at every pixel (x,y).

most common LCTF system (Lyot design) transmits a narrow-band wavelength by applying a varying voltage on a polarizable liquid crystal mounted between two linear polarizers (Fig. 3C). Usually a few stages are needed to achieve high resolution which reduces the total transmission within the filter's passband. An AOTF uses a crystal such as Tellurium dioxide (TeO_2) on which acoustic waves are applied (Fig. 3D). At each frequency of the acoustic waves, the crystal deforms to a grating with a specific period and therefore transmits a different wavelength in a given direction. These types of filters capture a full spectral image by measuring one image at a time but each time at a different wavelength. They have the advantage that a user-selectable number of wavelength images can be acquired as well as the flexibility to choose an optimal exposure time for each separate wavelength. On the other hand, the spectral resolution is usually hardware-dependent and, for a given system, cannot be changed. See, for example, the review by Gat (12).

Spatial-Scan Methods

In this method, the dispersion of light is achieved by using either a grating or a prism (Fig. 3E). These are very common in single-point spectrometers but, when used for

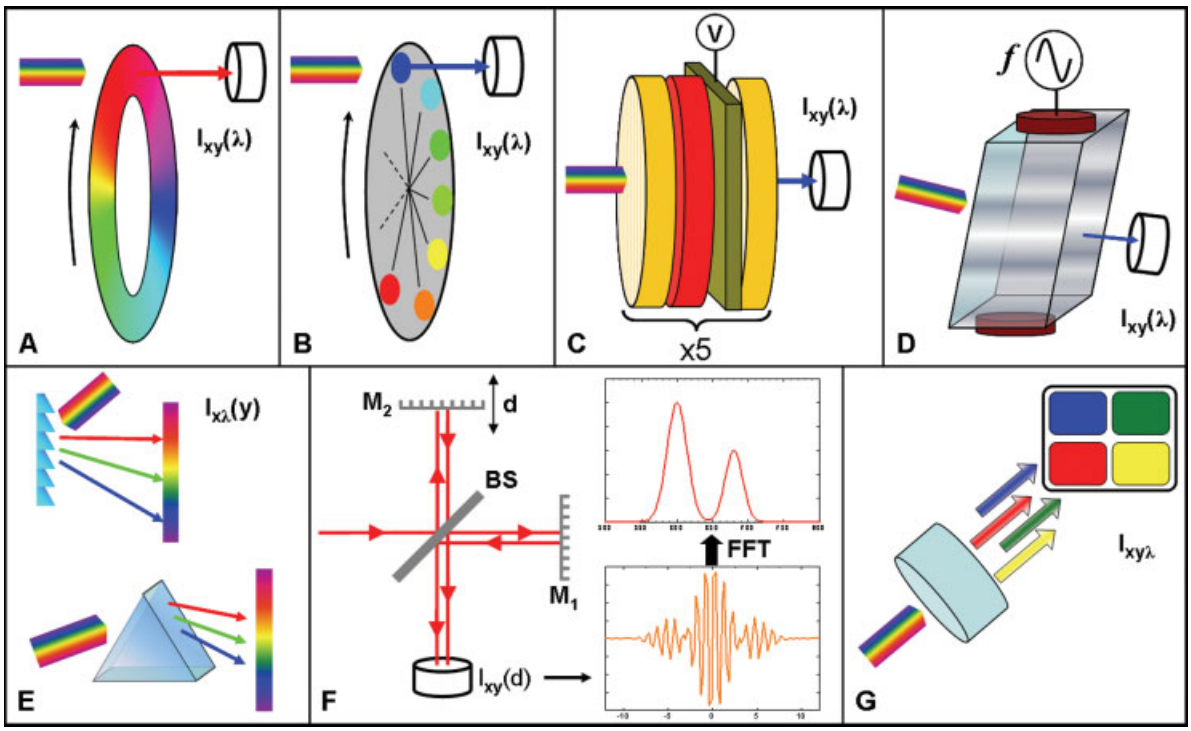

FIG. 3. Various methods of spectral imaging systems. They can be divided into four main methods: wavelength-scan (**A–D**), spatial scan (**E**), time scan (**F**) and "compromise" methods (**G**). In wavelength-scan methods, the whole image is measured one wavelength at a time. This can be realized using either a circular variable filter (A), a set of filters (B), a liquid crystal variable filter (C) or an acousto-optic variable filter (D). Spatial-scan methods use a dispersion element, either a grating or prism (E) and the image has to be scanned along at least one axis. There are also confocal microscopes that use a dispersive element and scan the image point by point. In time-scanning method (F), the whole image is measured after passing through an interferometer (or other optical elements). In order to calculate the spectrum at each pixel a mathematical transformation has to be carried out, for example, a Fourier transform. In "compromise" methods (G) only a few spectral ranges are measured and the FOV is limited, but the measurement is fast.

spectral imaging. Only one line of the object can be measured at a time. This requires one to scan the object line-by-line to collect the entire spectral image. The data is therefore collected as $I(x,\lambda)$ and then scanned along y (13). These methods have an advantage when the measured object is moving linearly and can be applied, for example, while scanning a Papanicolau-smear sample on an automated stage. On the other hand, the scanning mechanism is required even if it is not an intrinsic part of the optical system.

It is also possible to measure the spectral image with a confocal microscope which scans the object point-by-point with a photomultiplier detector. This is done by passing the light through a prism or grating in the optical path to the detector (or using a line-detector) (14). Such methods are advantageous when the confocal advantage is needed (e.g., thick samples). On the other hand it uses a significantly smaller number of detector elements for the acquisition relative to CCD-based methods. Therefore, a longer acquisition time is required in comparison to the CCD-based systems in order to achieve the same SNR.

Time-Scan Methods

Another method is based on measuring data that is a superposition of the spectral or spatial information and therefore requires the transformation of the acquired data to derive the spectral image. One of these methods is Fourier spectroscopy (15,16), see Figure 3F. In this method there are no filters and the spectrum is measured by using the interference of light. An interferometer (Fig. 3F) is a system that splits a beam of light into two beams, creates an optical path difference (OPD) which is also a time delay between them (Mirror M_2 in Fig. 3F), and joins the beams back again to interfere at the detector. When the intensity is measured as a function of many OPDs, it forms a pattern called an interferogram that is specific to the tested spectrum. The interferogram is then Fourier-transformed in order to determine the spectrum. Figure 3F shows a Michelson interferometer but other interferometers, such as Sagnac, exist that have stability advantages (16). This method has the advantage that the intensity at each wavelength is collected throughout the whole duration of the measurement. It also allows selecting the required spectral resolution without any changes to the hardware, simply by setting specific acquisition parameters. On the other hand, the full spectrum must be collected even if only a small number of points spread along the spectral range are needed.

Another method that is related to time-scanning methods is based on the Hadamard transform (17). This method uses an imaging spectrometer equipped with a CCD and special optics. A spatial light modulator compresses the whole 2D image onto the slit of the imaging spectrometer and allows blocking any set of points from the image. By measuring many 2D images, each of which contains a superposition of spatial and spectral information and performing a Hadamard transformation, the spectral imaging information can be retrieved.

Methods That Compromise Spatial or Spectral Parameters

In this approach, a compromise is sought for the simultaneous measurement of spectral and spatial parameters. These methods are suitable for high-speed spectral imaging measurements which are crucial in several applications such as detecting fast metabolic processes. The simplest method is to select a smaller part of the FOV and project it multiple times on the same CCD, each one through a different filter (18) (Figure 3G). As shown, the FOV reduces four-fold and only four spectral ranges are measured. A related approach has been taken in flow cytometry where a dispersion element projects six emission images onto a time-delayed integration CCD whose pixel clock rate is synchronized with the flow stream (19). Another such method is computed-tomography (20) where a holographic disperser is designed to project spectral-spatial information on a single CCD array. The spectral image itself has to be reconstructed from the raw data. Here too, the spatial resolution and FOV are traded off for the spectral information.

Spectral images usually measure the emission (or transmission) from the samples, but excitation spectra can also be obtained by placing the system on the excitation optical port. For transmission measurements, such a method provides similar information, but it is different for fluorescence. Dickinson et al. (21) has extended the excitation method to multiphoton excitation (22) and has shown how it can be used to eliminate autofluorescence and distinguish dyes with similar emission spectra.

SPECTRAL IMAGING CHALLENGE: INFORMATION VERSUS TIME

A spectral image contains significantly more information and data than a single color image and, thus, takes longer to acquire. When comparing the total acquisition time of different methods, it should be based on a comparison of similar images quality or SNR.

Theoretically, the ideal system includes many shot-noise limited detectors that can measure simultaneously the entire spectral image. If, in addition, we could tune the spectral-range sensitivity of each one of these detectors, it would provide the ideal system. Such a detector may look like a cubical structure (Fig. 2) where each box is a detector.

So far, no such detector is available. The total acquisition time continues to depend on the sequential number of times that data has to be collected. It is clear, however, that the larger the number of detector elements that can be used in parallel, the shorter the measurement time will be.

As an example, assume that it is only required to measure an image with three spectral components which are in the blue, green, and red spectral ranges. If a gray-level CCD is used, it requires an acquisition of three images. There are also sensors that allow one to capture three color ranges simultaneously (23), such as from Foveon (Santa Clara, CA). The Foveon sensor captures the three colors simultaneously with full coverage of the image (full "fill factor"). Similar effect is achieved also with a three-

chip color CCD that uses dichroic mirrors to capture the colors simultaneously. Such devices require only a single acquisition relative to a gray-level CCD that uses three filters sequentially and will lead to an improvement of the SNR (assuming the same quality of the detector elements).

On the other hand, because we have chosen the number of colors and the associated wavelengths ahead of time, data are acquired that can answer only a specific question (e.g., measuring aneuploidy in cancerous cells). Therefore, a fair comparison of different acquisition methods should be based on the time it takes each method for acquiring enough information for answering the relevant question. The problem can be formulated as follows:

In a given amount of time, what is the optimal set of spectral-component images that enables one to interpret the data with a given level of accuracy.

Time limitation can be critical for different reasons: high throughput that is required in many applications, photobleaching in fluorescence, or phototoxicity.

Methods for answering the question formulated above have been treated before. They depend on the specific spectra that have to be separated and in the case of fluorescence, the complexity is even higher. The fluorochromes have to be excited at certain spectral ranges, which limits the spectral ranges that are available to detection (24). Zimmermann et al. (18) have formulated the problem for the case of live-cell spectral imaging which introduces even stronger restrictions on the acquisition times. Neher and Neher (25) have developed a more general methodology for solving the problem for the case of multiple fluorochromes and also take into account bleaching effects.

Two of the applications described later for spectral unmixing demonstrate two extreme solutions for quantitatively analyzing overlapping fluorochromes, one that uses only two matched filters and the other that measures a full spectrum.

SPECTRAL IMAGE PROCESSING

A spectral image usually contains hundreds of thousands of spectra, one for each pixel. The data files are therefore too big and complex to interpret visually and require a comprehensive set of tools for displaying spectral-image data, processing them and presenting the results (26).

The analysis of spectral images may be performed based upon either the spectral features or the image features or both.

Modern image processing methods and algorithms are, in general, adequate and relevant for spectral imaging as well. For a review, see Young et al. (27). Spectral analysis is by itself a broad field. A few of the more basic algorithms in spectral imaging are described later. A specific application requires specific analysis methods that combine both spectral and image analysis algorithms. An example of such a combined image and spectral analysis is described by Schwartzkopf et al. (28).

LINEAR DECOMPOSITION (FLUORESCENCE)

The linear decomposition algorithm, also termed spectral unmixing (29), is based on the assumption that the measured signal from each color is linearly proportional to the concentration of that color in the object. This assumption is correct when the absorption and fluorochrome concentrations are low; otherwise correction terms should be used. The linear decomposition algorithm is well known, simple to implement and very fast on modern computers (30).

Assume that few fluorochromes are used in an experiment, and each one labels a different entity. The fluorochromes may be found either separately or as a mixture in the image. The linear decomposition algorithm finds the amount of each fluorochrome at each pixel. In its simplest form, the algorithm requires measuring and saving the emission spectra of the distinct fluorochromes prior to the actual analysis with the same instrument conditions (such as the microscope filter-cube). It also requires that the separated spectra are distinguishable from one another, and are linearly independent (none of the spectra can be written as a linear combination of the others). This is not a trivial assumption as the linearity criteria may be disrupted by energy transfer between co-localized fluorochromes (31). Energy transfer may lead to reduction of the fluorescence intensity of the donor fluorochromes, slight change in its spectrum, and increased intensity of the acceptors. Nevertheless, the effect is usually small but should be considered, especially when using fluorochromes that are efficient energy-transfer pairs.

The algorithm and result of linear decomposition are demonstrated in Figure 4 where three different ratios of two fluorochromes are used (1:1, 1:2, and 2:1). If the reference spectra are known, the algorithm finds the amount of each of the single dyes so that the addition of them all gives a spectrum that is the most similar to the measured spectrum. In case the reference spectra are not known, algorithms such as similarity mapping can be used (Fig. 5).

Linear decomposition is used also in spectral karyotyping described later by using a set of five different spectra (Fig. 6) and deducing the correct mixture of fluorochromes at each pixel. The results are used to identify the chromosome material at each pixel and the results are displayed in classification colors (Fig. 7, right). It was used also for live-imaging analysis as described later to separate the contribution of Histone-GFP and YFP in the Golgi (Fig. 8, see the separated contributions in 8D and 8E) by using the reference spectra of GFP and YFP that are considerably overlapping.

It can also be used in bright-field microscopy, though it requires some more preprocessing as described later (spectral unmixing for tissue section analysis). Figure 9 demonstrates the usage of the spectra for separating the contributions of hematoxylin and eosin.

For simplicity, consider the spectrum at a single pixel. Each spectrum of a pure fluorochrome is described as $I_i(\lambda)$ where $i = 1,2 \ldots N$ represents the index of a fluorochrome. The spectrum $I_i(\lambda)$ can be viewed as a vector with dimension that is equal to the number of points in the spectrum, M. The concentration of each fluorochrome (relative to the concentration of the measured references) can be described by C_i and the measured spectrum can be written as $I(\lambda) = \sum_i C_i \cdot I_i(\lambda)$. This can

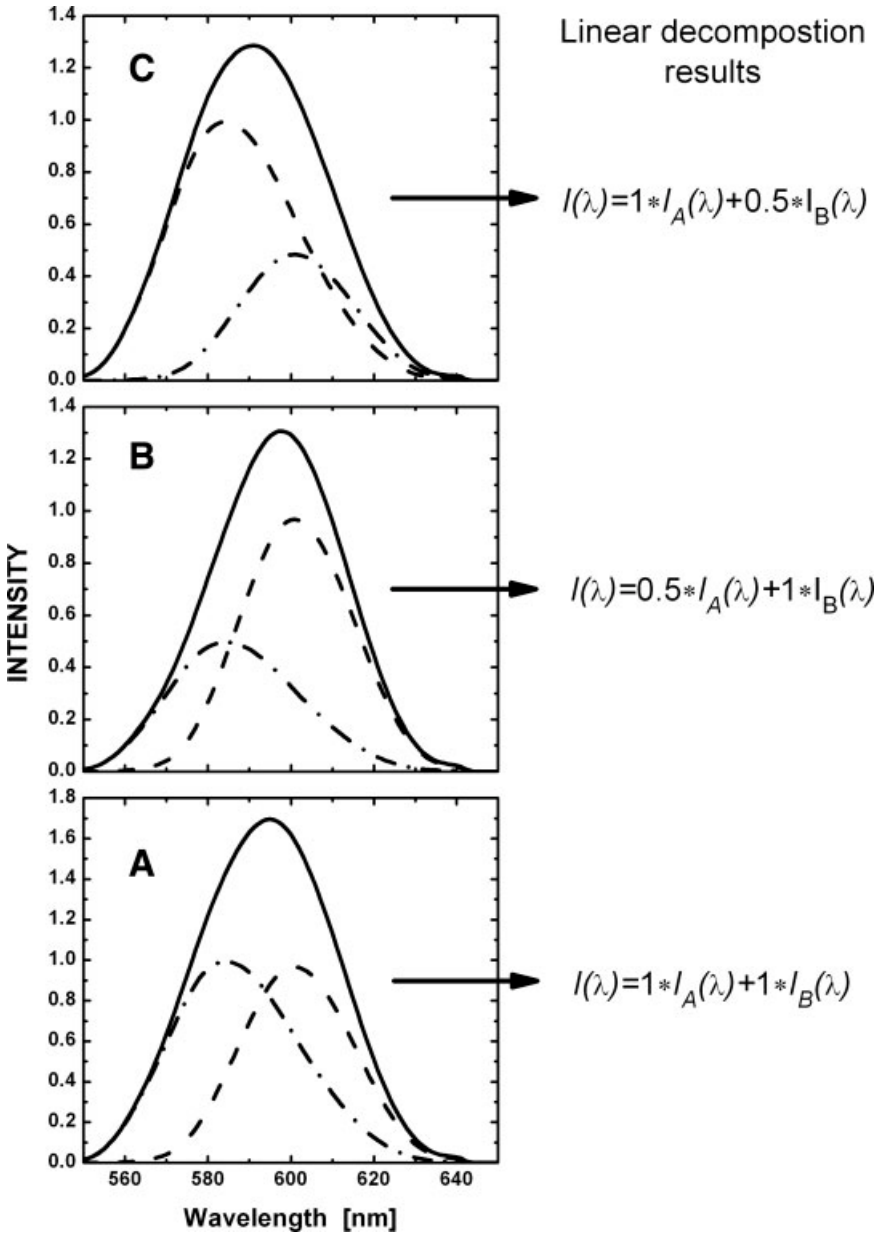

FIG. 4. Demonstration of the linear decomposition algorithm. Dash and dash-dot graphs represent the spectra of two different dyes A and B. When mixed together, the actual measurement (solid line) is the addition of these two. The linear decomposition algorithm finds the relative contribution (equations on the right). (**A**) Mixture of 1:1 ratio. (**B**) Mixture of 1:2 and (**C**) 2:1 ratio.

be written in a matrix form where **F** is the matrix of the references spectra,

$$\begin{bmatrix} I(\lambda_1) \\ I(\lambda_2) \\ \vdots \\ I(\lambda_M) \end{bmatrix} = \begin{bmatrix} I_1(\lambda_1) & I_2(\lambda_1) & \cdots & I_N(\lambda_1) \\ I_1(\lambda_2) & I_2(\lambda_2) & & \\ \vdots & & \ddots & \\ I_1(\lambda_M) & \cdots & & I_N(\lambda_M) \end{bmatrix} \times \begin{bmatrix} C_1 \\ C_2 \\ \vdots \\ C_N \end{bmatrix}$$

$$= \mathbf{F} \times \begin{bmatrix} C_1 \\ C_2 \\ \vdots \\ C_N \end{bmatrix} \quad (1)$$

If $M \geq N$ (i.e., the number of points in the spectrum is larger than or equal to the number of fluorochromes), it is possible to find the left-inverse matrix of **F**, $\mathbf{F}^{LI}$ so that the multiplication $\mathbf{F}^{LI} \times \mathbf{F}$ gives an identity matrix. The values of fluorochrome concentrations at each pixel can then be calculated by:

$$\begin{bmatrix} C_1 \\ C_2 \\ \vdots \\ C_N \end{bmatrix} = \mathbf{F}^{LI} \times \begin{bmatrix} I(\lambda_1) \\ I(\lambda_2) \\ \vdots \\ I(\lambda_M) \end{bmatrix} \quad (2)$$

Note that $\mathbf{F}^{LI}$ depends only on the reference spectra, and can be calculated and stored before the actual measurement. Because of noise, the measured data is not a perfect

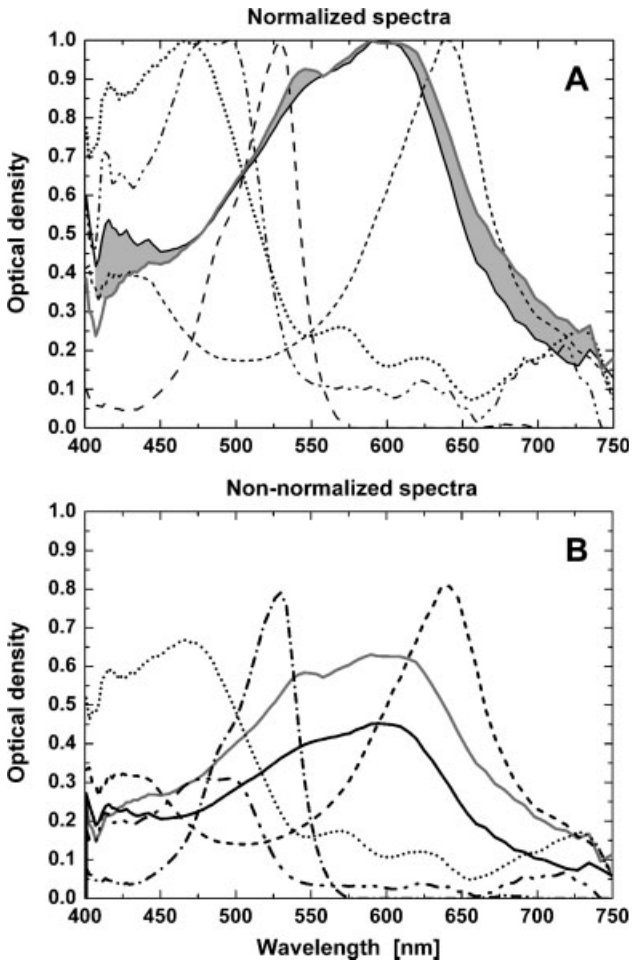

FIG. 5. Similarity mapping algorithm. The absorption spectra of tissue stains (black) and a tested spectrum (gray) are shown. (**A**) Normalized spectra. The area between the tested graph and the most-similar one is filled (light-gray). It is calculated for all the references (**B**) Spectra as measured.

linear combination of the references and therefore the calculation can only provide an estimated solution for the **C** values. The quality of the solution can be tested by comparing the measured spectrum with the predicted spectrum, $I'(\lambda) = \mathbf{F} \times \mathbf{C}$. The vector **C** must have only positive values, and therefore a constrained algorithm must be used that prevents a solution with negative values. One possible method is to find the vector C that minimizes ε, the least square normal, $\varepsilon = |\mathbf{F}^{LI} \cdot \mathbf{C} - \mathbf{I}(\lambda)|^2$ such that $C_i \geq 0$ for every i (32).

SIMILARITY MAPPING

In some cases, such as histological stains used with tissue section, the measured spectra are a result of a complex interaction of the stains with the sample and it may not be possible to isolate the different components that contribute to the spectrum. Therefore, the linear decomposition method cannot be used.

In such cases, a similarity mapping algorithm can be important. It is based on information provided from the sample itself or similar samples. In this method, the user identifies unique regions from the sample such as different tissue types. The average spectrum from each of these regions is calculated and stored in a library as $I_i(\lambda)$ where i is the index of each spectrum.

The similarity mapping algorithm tests the degree of similarity of each spectrum in the image with each one of the reference spectra (Fig. 5). A tissue section was stained with a few stains and the spectral image of it was measured. Five different tissue structures were identified and their spectra were saved as references (Fig. 5, black lines). Then, a tested tissue is measured; one of its spectra is shown in gray color. When analyzing the image, it is important to know what is the feature represented by the spectrum. This can be done by comparing the tested spectrum and the saved references. A possible method is to calculate the area in between the measured spectrum and each one of the reference spectra. A large area means the spectra are different and small area means that they are similar.

More commonly, a least-square algorithm is used. The tested spectrum is defined as $\bar{I}(\lambda)$ and the n-dimensional distance for each reference is calculated, $D_i = \sqrt{\Sigma_\lambda (I_i(\lambda) - \bar{I}(\lambda))^2}$. The reference spectrum i that has the smallest distance D_i is selected as the most similar. Usually, the spectra are normalized to their area (or peak intensity), so that only spectral shape differences are tested.

The calculation with the five different spectra in Figure 5A gives for D_i the values of 0.07, 1.04, 0.91, 0.59, and 0.84, which means that the first spectrum (solid line) is the most similar, as can be easily seen.

Another variation of similarity mapping is to calculate the M-dimensional angle between each reference spectrum and the tested spectrum (M being the number of points in the spectrum). If we define each one of the reference spectra as a vector $\mathbf{I}_i = (I_{i,\lambda 1}, I_{i,\lambda 2} \ldots I_{i,\lambda n})$, i being

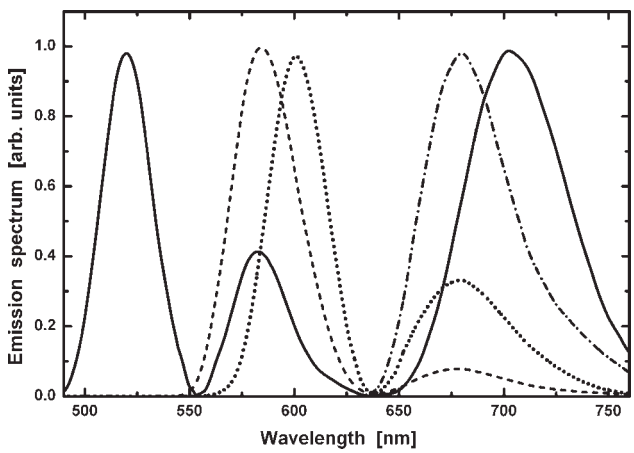

FIG. 6. Spectra of the five fluorochromes that are used for SKY as measured with the SpectraCube system through a triple dichroic SKY filter cube. Typical fluorochromes (or alike) are FITC (solid line), Rhodamine (dash), Texas Red (dot), Cy5 (dash-dot) and Cy5.5 (solid gray). The spectral differences allows one to use many different combinations of these dyes.

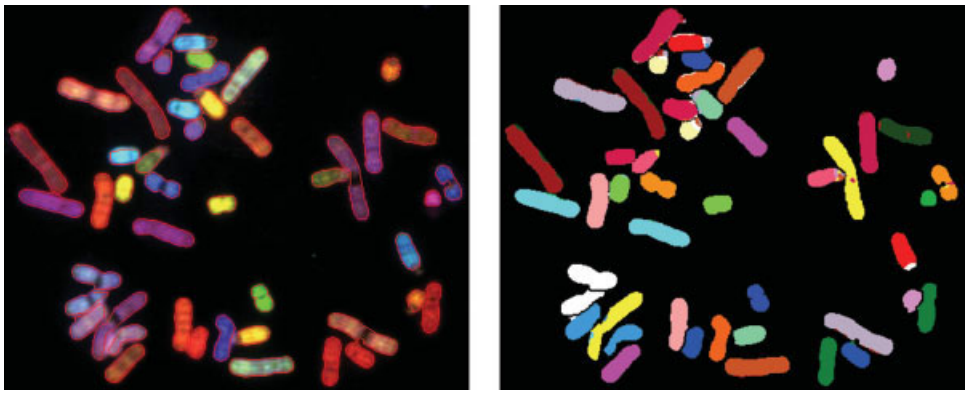

FIG. 7. SKY measurement and classification results. Human metaphases are hybridized with a SKY kit that contains the appropriate combinatorial labeling for each chromosome (Applied Spectral Imaging, Migdal HaEmek, Israel). The measured spectral image is translated to display-colors (left). The SkyView software analyzes the images based on both the spectrum and the image information. Images are segmented (left) and classified based on a reference library and the known fluorochrome combinations of each chromosome. The results are shown in classification colors (right image).

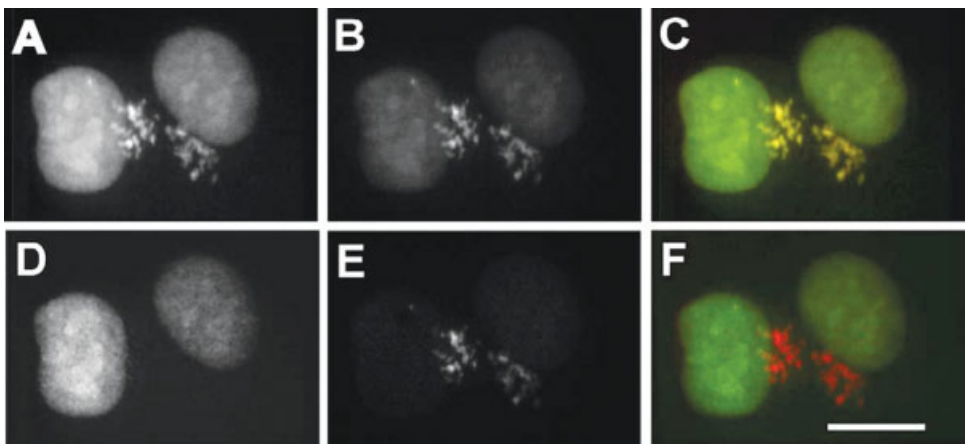

FIG. 8. **A–F:** In vivo imaging of EGFP and YFP fusion proteins using 488 nm excitation and simultaneous detection in two channels (505–530 and 530–565 nm). The images show the projections of an acquired 3D (x,y,z) stack before (A–C) and after (D–F) the mixing. A: Detection at 505–530 nm. B: Detection at 530–565 nm. C: Overlay of the channels in (A) and (B). D: Histone-GFP in the nucleus. E: YFP in the Golgi. F: Overlay of (D) and (E). The figure reproduced with kind permission of R. Pepperkok (18).

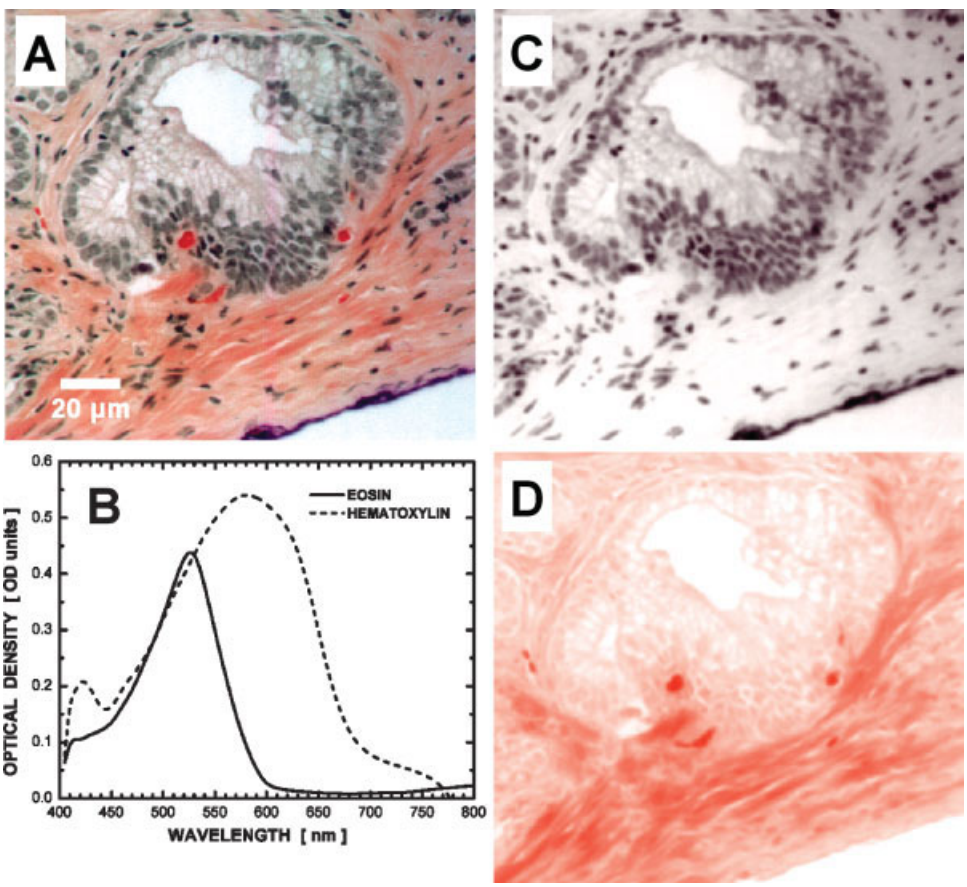

FIG. 9. Spectral unmixing applied to a pathological prostate tissue section stained with hematoxylin and eosin. (**A**) Color image as created from the spectral image. It is similar to the visual image as seen through the microscope. (**B**) Optical density spectra of hematoxylin and eosin as measured on reference slides. (**C**,**D**) Results of the spectral unmixing. They show how the tissue section would have looked if it were stained with only hematoxylin (C) or only eosin (D). Tissue section courtesy of Dr. Farhad Moatamed, West Los Angeles Veterans Administration Hospital, Los Angeles, CA, USA.

the index of the reference spectrum and the tested spectrum as **I**, then the angle α_i can be calculated by

$$\alpha_i = \cos^{-1}\left(\frac{\mathrm{I}_i \cdot \mathrm{I}}{|\mathrm{I}_i| \cdot |\mathrm{I}|}\right) = \cos^{-1}\left(\frac{\sum_\lambda I_i(\lambda) \cdot I(\lambda)}{\sqrt{\left(\sum_\lambda I_i(\lambda)\right)^2} \cdot \sqrt{\left(\sum_\lambda I(\lambda)\right)^2}}\right) \quad (3)$$

The smaller the angle, the more similar the spectra.

SPECTRAL UNMIXING FOR TRANSMISSION (BRIGHT FIELD) MEASUREMENTS

This algorithm is similar to the linear decomposition algorithm described before, but is specific to bright field (transmission) microscopy. The method is somewhat more complex because the important information in this experiment is the absorption at each point that must be calculated from the measured transmission data.

The absorption spectrum of a dye molecule is, to a good approximation, linearly dependent on the concentration of the molecules c, the light path length in the sample l, and on the extinction coefficient $\varepsilon(\lambda)$ that describes the probability of one molecule to absorb light quanta at wavelength λ. This approximation may fail if the absorption is relatively high, but this case will not be discussed here. The absorption can be found by using the Beer-Lambert law:

$$I(\lambda) = I_0(\lambda) \cdot 10^{-\varepsilon(\lambda)\cdot c \cdot I} \quad (4)$$

where $I(\lambda)$ is the measured spectrum (that is the transmission measured through the sample) and $I_0(\lambda)$ is the spectrum of the light source as measured with the same conditions without the sample. These spectra would be defined here in dimensions of flux, i.e. photons/cm^2/s/wavelength [cm^{-2} s^{-1} nm^{-1}].

An index j is used to distinguish different absorbing molecules, $\varepsilon_j(\lambda)$. The dimensionless term at the exponent of Eq. (1) is called the absorbance,

$$\text{Absorbance} = \varepsilon(\lambda) \cdot c \cdot l \quad (5)$$

As one can see, the absorbance is linear with the number of molecules along the optical path in the sample. There are different unit-conventions for this equation. We use the extinction coefficient in molar density [M^{-1} cm^{-1}] and the molecules concentration c in mol/L (33) (M, the molar, has units of mol/L).

An absorbance of 0.3, 1, and 2 relates to absorption values of 50, 90, and 99%, corresponding to transmission of 50, 10, and 1%. With typical spectrometric instrumentation, the absorbance can be measured over at least four orders of magnitude but it is reduced with imaging applications due to higher noise levels.

When the sample contains few absorbing stains, the transmission spectrum has a complex structure (34). The absorbance depends on the different absorbers, $A(\lambda) = \sum_i \varepsilon_i(\lambda) \cdot C_\mathrm{i} \cdot l_i$, which is similar to the case of fluorescence, with the preliminary step of calculating it from the measured transmission, $A(\lambda) = -\log(I(\lambda)/I_0(\lambda))$. The division operation can insert significant amounts of noise especially where there is a low signal. This requires that we consider excluding the "tails" of the spectra where the intensity is weak.

If the absorption spectra of the different stains are measured separately, it is possible to calculate the concentration of each stain in each pixel of the image. It also requires that the absorption spectra of each stain do not change locally on the sample, a condition which is usually met.

A few studies have indicated the applicability of spectral imaging for multiple color bright-field applications. See, for example, the work by Ornberg et al. on histological sections (35) and Macville et al. (36) on tissue sections and cervical smears using different types of stains.

Some of the stains, for example diaminobenzidine, are actually scattering polymers, not absorbers. The consequence of this is that the quantitative analysis of such stains may not be correct because the linearity assumption does not hold.

NONSUPERVISED METHODS AND PRINCIPLE COMPONENTS ANALYSIS

The spectral analysis methods described earlier belongs to a family of algorithms called supervised classification methods. Such methods require reference input by the user, such as a spectral library of the expected classes. In contrast to that, nonsupervised classification methods do not require reference spectra as an input. In these methods, a mathematical algorithm determines the different groups of spectra based on their spectral properties. This approach is frequently described as clustering and may involve only a minimum of a priori information such as the number of stains that have been used. The user should still test the validity of the results and, at some point, tune various parameters.

One of those algorithms is principle component analysis (PCA). It uses statistical analysis of the whole data set (all the spectra in the image) and finds the similarities and differences in the data (37). PCA does not require spectral reference curves and the main features of the data are automatically found during the analysis. The statistical analysis finds a small set of spectra that represents the whole dataset. The first spectrum in the set is a spectrum that contributes the most to the spectra in the image; the second one contributes less, and so on.

The principle spectra that are found by PCA represent special classes of the measured objects (e.g., a cancer versus a normal cell).

APPLICATIONS

Spectral imaging provides tools that are useful for a variety of applications. The spectral information allows detecting and distinguishing among many different fluorochromes even if they have a similar color or overlapping spectra. This permits one to label different entities in a

sample simultaneously and to quantitatively analyze each entity. The spectral information can also be used to distinguish the "real" stain from unwanted contributions such as autofluorescence that are physically significant in some cases but biologically irrelevant. It is also possible to study spectral changes which are indicative of a process that the sample experiences. A few of the applications are described in the following.

Observation of Multiple Colors

In many cases, there is a need to observe simultaneously few or many dyes (both fluorescence and bright field) in order to identify a number of proteins, genes or organelles and their co localization. Even though there are many different dyes, many of them have a similar color so that only a few can be distinguished by eye or by a simple color filtering technique. Spectral imaging enables to overcome this obstacle.

In fluorescence, it is necessary to excite all the dyes, but the emission spectral range cannot overlap with the excitation range. This means that part of the spectral range that is used for excitation cannot be used for detection. To overcome these difficulties, multiband filters are used so that more than one fluorochrome can be detected in each band of the filter. This usually prevents using two dyes for which the excitation of one overlaps with the emission of the other.

Spectral karyotyping. An example of such an application is spectral karyotyping or SKY (15,38,39), probably the most wide-spread application of spectral imaging to date. SKY is based on fluorescence in situ hybridization (FISH). Five different fluorochromes are used (Fig. 6) to label each one of the 24 human chromosomes (or other species). Each chromosome is labeled with a different combination, as an example, chromosome 2 is labeled with Cy5.5 and chromosome 3 is labeled with FITC, Rhodamine, Cy 5 and Cy5.5. With 5 fluorochromes, there are $2^5-1 = 31$ different possible combinations. As a result, the spectra that are measured at each pixel are a weighted combination of the single-fluorochrome spectra that are shown in Figure 6.

Spectral images are usually acquired with a 63× or 100× objective lenses with high NA (1.3–1.4) in the range of 450–780 nm and with a spectral resolution of 10 at 500 nm. The spectral data is displayed as an RGB image where the green fluorescence is displayed in blue, orange and red is displayed as green and the far-red is displayed as red (Fig. 7, left). The spectral images are then processed and analyzed with spectral and imaging algorithms. The spectral image is segmented (Fig. 7, left) and each pixel is classified based on its spectrum, a reference library of the five fluorochromes spectra and a table of the combination labels of each chromosome (Fig. 7, right). The classification results are displayed in classification colors where each color represents a different chromosome. The classification can be further tested and analyzed by observing the spectrum at each pixel, comparing it to the references and testing the fluorochrome-mixtures that are found by the linear decomposition algorithm that is used by the system. The high specificity of the acquired spectral data enables a successful classification in the vast majority of the slides preparation, even on complex tissue sections. It is therefore used intensively for both diagnostics and research (15,38,39).

Similar approaches called M-FISH and COBRA-FISH have been developed by using a set of matched filters instead of measuring the spectral images and provides similar information (40,41). In another approach, seven color analyses of immunofluorescence-stained tissue samples have been performed (42) with a Fourier-based spectral imager by acquiring spectral images with three different filter sets. Pautke et al. used a similar method for observing eight calcium-binding fluorochromes for studying bone-formation (43). Gao et al. have used spectral imaging for observing bioconjugated quantum dots for cancer targeting in vivo in mice, and have shown the power of spectral imaging to eliminate autofluorescence signal (11). Eight color immunofluorescence has been achieved by using a laser-scanning cytometer in combination with filter sets (44,45).

Live Cell Spectral-Imaging

A spectral image takes a long time to measure. For live-cell imaging, a compromise on the spectral resolution can provide an adequate solution, in contrast to the SKY method described earlier. The following example, based on the works published by Pepperkok and coworkers (18,46), was designed to allow fast multicolor time-lapse microscopy and fluorescence resonance energy transfer measurements in living samples. Even though it uses only a very few wavelength, we believe that such methods have the potential to be extended to full real-time spectral imaging. Nuclei were labeled with histone-EGFP and the Golgi complex with a Golgi-targeted YFP (two fluorescent proteins). Two filters were designed for measuring the emission from the image using simultaneous detection and subsequent emission unmixing (Fig. 8). The sample was excited at 488 nm with an ArKr laser and the fluorescence signal was split into two channels detecting the 505–530 nm and 530–565 nm range, respectively. The filters were selected based on prior knowledge of the individual fluorescent proteins' spectra. An emission beam splitter (DualView, Optical Insights, Tucson, AZ) was used for splitting the two spectral channels into two different areas of the CCD. Figure 8 shows projections of an acquired 3D stack (see caption).

Spectral Unmixing for Tissue Section Analysis

In bright field measurements, the full spectral range is available for detection; there is no need for selective spectral-excitation as in fluorescence. The signal is bright, the SNR is high, and there are, in general, no bleaching problems. On the other hand, mixtures of stains may have a complex spectrum and the more stains that are added, the more "brown" the sample gets, simply because of the large absorption of light by the many stains. This is the case in histological staining when multiple features have

to be detected. Spectral imaging can provide significant assistance.

Spectral unmixing allows one to analyze n stains (e.g., chromogens) in brightfield mode and calculate the concentration of each. Moreover, it allows one to separate the complex color-image into a set of single color images where each one of them shows the sample as if it were stained with only a single stain. It, therefore, has the advantage that many stains can be used simultaneously while it is still possible to visually analyze it as if it were stained with a set of single stains. By correlating the single-stain distribution, it also provides information on the co-localization of structures, proteins and other entities. The methods require that the absorption spectra of the chromogens that are used do not change significantly as a function of the local environment, a condition that has been tested and found to be correct.

Spectral unmixing requires three steps after the sample preparation and spectral image measurement. In the following example a pathological prostate tissue section was stained with hematoxylin and eosin (Fig. 9). Spectral images were measured with the SpectraCube SD200 system (Applied Spectral Imaging, Migdal HaEmek, Israel) in the range of 400–800 nm and with a spectral resolution of 10 at 500 nm on a bright field Nikon Eclipse E800 microscope (20× objective lens, NA = 0.75). The light source was a 100 W 12 V tungsten halogen lamp with a BG38 filter to block infrared light.

Spectral unmixing includes the following three main steps:

1. The single stains and light source spectra are measured on a reference known sample, such as a set of consecutive tissue sections, and the absorbance of each one, $A_i = \varepsilon_i(\lambda) \cdot c_i \cdot l_i$ is calculated and saved in a library (Fig. 9B). Then, the spectral image of the sample is measured (Fig. 9A) and the concentration of each stain is calculated based on the formalism described earlier (image processing section). This provides the concentration of each stain at every pixel. Figure 9A shows a color image that is recreated from the spectral image. It is similar to the image that would have been measured with a color camera.
2. Using α_i, it is possible to calculate the absorption spectrum that will result if the sample would have been stained with only a single stain, $I_i^*(\lambda) = \alpha_i \cdot \varepsilon_i(\lambda)$. This information is now used to calculate the transmission spectrum that would be measured if only a single stain were used, $T_i^*(\lambda) = I_0(\lambda)10^{-\alpha_i \cdot \varepsilon_i(\lambda)}$.
3. The color image is calculated from the transmission spectrum by using the three visual color response functions (for red green and blue) and integrating the intensity for each color. This allows the display of the i different color images for each stains (Figs. 9C and 9D).

Spectral unmixing was performed using the SpectraView™ software after measuring the spectral images with the SpectraCube™ (Applied Spectral Imaging) on a hematoxylin and eosin stained prostate tissue section with reference spectra acquired from serial-section single-stained images (Fig. 9). Three reference spectra were used: hematoxylin, eosin, and the white background spectrum (transmitted light source spectrum at the plane of focus). Figure 9B shows the absorption reference spectra (as defined above) measured in optical density units. After conversion to spectral optical density data (as described earlier), the spectral data were unmixed. Repeating previous arguments, conversion to optical density is necessary because the amount of any dye is linearly proportional to the optical density value but is not linear with respect to the R, G, or B intensity values. This is not crucial for hematoxylin or eosin neither of which is intended to be a quantitative dye-but it is crucial to obtaining correct dye amounts from immunohistochemistry stains or from DNA quantitation using the Feulgen reaction.

In Figure 9, the prostate cancer tissue is in the center of the image. The bottom right has connective tissue that is heavily stained with eosin. Eosin is present in the cytoplasm and the nuclei of every cell. Visually, nuclear eosin is masked by the presence of hematoxylin but spectral unmixing reveals the nuclear eosin.

DISCUSSION AND CONCLUSIONS

Spectral imaging is an active field, made possible through the advances in CCD detectors, dispersion optics, and spectral image processing algorithms. A number of systems are now available and spectral imaging is a well established technique. In this article, a few of the optical methods, image processing algorithms, and measurement methods have been described and presented with a few examples.

With existing detectors, which are at most 2D in nature, a spectral image can be measured only by acquiring multiple images of the object. This makes the acquisition relatively slow and inappropriate for applications that require high-speed measurements or samples that cannot tolerate excessive exposure to light. This has led to the development of methods that compromise spectral and spatial requirements, but still provide the desired information. We believe that further technological advances will lead to the development of new architectures for detector systems that will allow significantly faster spectral image measurements.

Spectral imaging can be used in imaging modes such as fluorescence and transmission. Each of these, however, requires a different analysis and interpretation approach.

Still more imaging modalities and the associated applications will be included in the coming years, broadening the practical usage of spectral imaging.

ACKNOWLEDGMENTS

We would like to thank Dr. R. Pepperkok (Advanced Light Microscopy Facility, European Molecular Biology Laboratory, Heidelberg, Germany) for providing the images for Figure 8 and allowing us to present part of his work. We thank Dr. Farhad Moatamed (West Los Angeles Vetrerans Administration Hospital, Los Angeles, CA) for providing us with the prostate tissue sections. We thank

Applied Spectral Imaging for providing the images measured with the SpectraCube system and analyzed with SpectraView and SKYVIEW.

LITERATURE CITED

1. Stelzer EHK. Contrast, resolution, pixelation, dynamic range and signal-to-noise ratio: Fundamental limits to resolution in fluorescence light microscopy. J Microsc 1997;189:15–24.
2. Newton I. Opticks (1704). Mineola: Dover; 1987.
3. Voltaire F-MA. Éléments de la philosophie de Newton; 1738.
4. Bohr N. On the constitution of atoms and molecules. Philos Mag 1913;26:1–25,476–502,857–875.
5. Schrödinger E. An undulatory theory of the mechanics of atoms and molecules. Phys Rev 1926;28:1049–1070.
6. Stuart BH. Infrared Spectroscopy: Fundamentals and Applications. Ando DJ, editor. Chichester: Wiley; 2004.
7. Smith E, Dent G. Modern Raman Spectroscopy, a Practical Approach. Chichester: Wiley; 2005.
8. Wyatt CL. Infrared spectrometer: Liquid-helium-cooled rocketborne circular-variable filter. Appl Opt 1975;14:3086–3091.
9. Miller PJ. Use of tunable liquid crystal filters to link radiometric and photometric standards. Metrologia 1991;28:145–149.
10. Shonat R, Wachman E, Niu W, Koretsky A, Farkas D. Near-simultaneous hemoglobin saturation and oxygen tension maps in mouse brain using an AOTF microscope. Biophys J 1997;73:1223–1231.
11. Gao X, Cui Y, Levenson RM, Chung LWK, Nie S. In vivo cancer targeting and imaging with semiconductor quantum dots. Nat Biotechnol 2004;22:969–976.
12. Gat N. Imaging spectroscopy using tunable filters: A review. Proc SPIE 2000;4056:50–64.
13. Sinclair MB, Timlin JA, Haaland DM, Werner-Washburne M. Design construction characterization and application of a hyperspectral microarray scanner. Appl Opt 2004;43:2079–2088.
14. Dickinson ME, Bearman G, Tille S, Lansford R, Fraser SE. Multi-spectral imaging and linear unmixing add a whole new dimension to laser scanning fluorescence microscopy. Biotechniques 2001;31:1272–1278.
15. Garini Y, Macville M, du Manoir S, Buckwald RA, Lavi M, Katzir N, Wine D, Bar-Am I, Schröck E, Cabib D, Ried T. Spectral karyotyping. Bioimaging 1996;4:65–72.
16. Malik Z, Cabib D, Buckwald RA, Talmi A, Garini Y, Lipson SG. Fourier transform multi-pixel spectroscopy for quantitative cytology. J Microsc 1996;182:133–140.
17. Hanley QS, Verveer PJ, Arndt-Jovin DJ, Jovin TM. Three-dimensional spectral imaging by Hadamard transform spectroscopy in a programmable array microscope. J Microsc 2000;197:5–14.
18. Zimmermann T, Rietdorf J, Pepperkok R. Spectral imaging and its applications in live cell microscopy. FEBS Lett 2003;546:87–92.
19. George TC, Basiji DA, Hall BE, Lynch DH, Ortyn WE, Perry DJ, Seo MJ, Zimmerman CA, Morrissey PJ. Distinguishing modes of cell death using the imagestream multispectral imaging flow cytometer. Cytometry A 2004;59A:237–245.
20. Descour MR, Volin CE, Dereniak EL, Gleeson TM, Hopkins MF, Wilson DW, Maker PD. Demonstration of a computed-tomography imaging spectrometer using a computer-generated hologram disperser. Appl Opt 1997;36:3694–3698.
21. Dickinson ME, Simbuerger E, Waters CW, Fraser SE. Multiphoton excitation spectra in biological samples. J Biomed Opt 2003;8:329–338.
22. Zipfel WR, Williams RM, Webb WW. Nonlinear magic: Multiphoton microscopy in the biosciences. Nat Biotechnol 2003;21:1369–1377.
23. Zimmer J, Knipp D, Stiebig H, Wagner H. Amorphous silicon-based unipolar detector for color recognition. IEEE Trans Electron devices 1999;46:884–891.
24. Garini Y, Gil A, Bar-Am I, Cabib D, Katzir N. Signal to noise analysis of multiple color fluorescence imaging microscopy. Cytometry 1999;35:214–226.
25. Neher R, Neher E. Optimizing imaging parameters for the separation of multiple labels in a fluorescence image. J Microsc 2004;213:46–62.
26. Garini Y, Katzir N, Cabib D, Buckwald RA, Soenksen DG, Malik Z. Spectral bio-imaging. In: Wang XF, Herman B, editors. Fluorescence Imaging Spectroscopy and Microscopy (Chemical Analysis Series). New York: Wiley; 1996. pp 87–124.
27. Young IT, Gerbrands JJ, van Vliet LJ. Image processing fundamentals. In: Williams DB, Madisetti VK, editors. The Digital Signal Processing Handbook, 1st ed. Boca Raton: CRC; 1998. pp 51.1–51.81.
28. Schwartzkopf WC, Bovik AC, Evans BL. Maximum-likelihood techniques for joint segmentation-classification of multispectral chromosome images. IEEE Trans Med Imaging 2005;24:1593–1610.
29. Zimmermann T. Spectral imaging and linear unmixing in light microscopy. Adv Biochem Eng Biotechnol 2005;95:245–265.
30. Mansfield JR, Gossage KW, Hoyt CC, Levenson RM. Autofluorescence removal multiplexing and automated analysis methods for *in-vivo* fluorescence imaging. J Biomed Opt 2005;10:41207.
31. Jares-Erijman EA, Jovin TM. FRET imaging. Nat Biotechnol 2003;21:1387–1395.
32. Lawson CL, Hanson RJ. Solving Least Squares Problems. Englewood Cliffs, NJ: Prentice-Hall; 1974.
33. Lakowicz JR. Principles of Fluorescence Spectroscopy. New York: Plenum Press; 1986.496 p.
34. Zhou R, Hammond EH, Parker DL. A multiple wavelength algorithm in color image analysis and its applications in stain decomposition in microscopy images. Med Phys 1996;23:1977–1986.
35. Ornberg RL, Woerner BM, Edwards DA. Analysis of stained objects in histological sections by spectral imaging and differential absorption. J Histochem Cytochem 1999;47:1307–1314.
36. Macville MV, Van Der Laak JA, Speel EJ, Katzir N, Garini Y, Soenksen D, McNamara G, de Wilde PC, Hanselaar AG, Hopman AH, Ried T. Spectral imaging of multi-color chromogenic dyes in pathological specimens. Anal Cell Pathol 2001;22:133–142.
37. Jolliffe IT. Principle Component Analysis. New York: Springer-Verlag; 2002.
38. Schröck E, du Manoir S, Veldman T, Schoell B, Wienberg J, Ferguson-Smith MA, Ning Y, Ledbetter DH, Bar-Am I, Soenksen D, Garini Y, Ried T. Multicolor spectral karyotyping of human chromosomes. Science 1996;273:494–497.
39. Schrock E, Padilla-Nash H. Spectral karyotyping and multicolor fluorescence in situ hybridization reveal new tumor-specific chromosomal aberrations. Semin Hematol 2000;37:334–347.
40. Speicher MR, Gwyn Ballard S, Ward DC. Karyotyping human chromosomes by combinatorial multi-fluor FISH. Nat Genet 1996;12:368–375.
41. Tanke HJ, Wiegant J, van Gijlswijk RP, Bezrookove V, Pattenier H, Heetebrij RJ, Talman EG, Raap AK, Vrolijk J. New strategy for multi-colour fluorescence in situ hybridisation: COBRA (COmbined Binary RAtio labelling). Eur J Hum Genet 1999;7:2–11.
42. Tsurui H, Nishimura H, Hattori S, Hirose S, Okumura K, Shirai T. Seven-color fluorescence imaging of tissue samples based on Fourier spectroscopy and singular value decomposition. J Histochem Cytochem 2000;48:653–662.
43. Pautke C, Vogt S, Tischer T, Wexel G, Deppe H, Milz S, Schieker M, Kolk A. Polychrome labeling of bone with seven different fluorochromes: Enhancing fluorochrome discrimination by spectral image analysis. Bone 2005;37:441–445.
44. Ecker RC, de Martin R, Steiner GE, Schmid JA. Application of spectral imaging microscopy in cytomics and fluorescence resonance energy transfer (FRET) analysis. Cytometry A 2004;59A:172–181.
45. Mittag A, Lenz D, Gerstner AOH, Sack U, Steinbrecher M, Koksch M, Raffael A, Bocsi J, Tárnok A. Polychromatic (eight-color) slide-based cytometry for the phenotyping of leukocyte NK and NKT subsets. Cytometry A 2005;65A:103–115.
46. Zimmermann T, Rietdorf J, Girod A, Georget V, Pepperkok R. Spectral imaging and linear un-mixing enables improved FRET efficiency with a novel GFP2-YFP FRET pair. FEBS Lett 2002;531:245–249.